NTNU
Norwegian University of
Science and Technology

Experiments in the wind turbine far wake for the evaluation of analytical wake models

Luis Garcia Salgado

Master's Thesis
Submission date: May 2017
Supervisor: Lars Sætran, EPT

Norwegian University of Science and Technology
Department of Energy and Process Engineering

Experiments in the wind turbine far wake for the evaluation of analytical wake models

Luis García Salgado

Department of Energy and Process Engineering, Norwegian University of Science and Technology, Trondheim, Norway

Abstract. Nowadays, not only the size of single wind turbines but also the size of wind farms is increasing. Understanding the interaction between the turbines and especially the wakes formed behind them are getting more important to further improve such wind turbine arrays. Consequently, new issues in wind energy research arise. An experimental wind tunnel study was conducted, in order to analyze and understand the far wake of a wind turbine. The experimental results were used to test if an analytical wake model derived by H. Schilichting for blunt bodies can be used to describe the velocity and width development in the far wake of wind turbines. Additionally, three analytical models for turbulence intensity were studied in order to investigate the turbulence intensity development downstream the turbine. The results of the evaluation show that the wake of a wind turbine agrees fairly well with the model according to Schlichting. The velocity deficit as well as the width in the wake behind the turbine, are found to deviate with around only 2% from the results obtained when the analytical model is applied. More spread results are obtained regarding the turbulence intensity predictions, however, accurate results can be achieved. Thus, it can be concluded that analytical wake models are well suited to estimate the velocity deficit, the width development and the turbulence intensity in the far wake of a wind turbine.

1. Introduction

Over the last decades, not only the size of single turbines but also that of wind farms has increased [1]. Consequently, it is getting more and more important to understand the interactions between single turbines in a wind farm to further improve the overall efficiency and reduced fatigue loads. Here, the wake formed behind the wind turbine plays a major role. This wake is mainly characterized by a velocity deficit and higher turbulence. Even though a lot of research has been devoted to the understanding of wind turbine wakes, it is not fully understood yet and further research in this topic is needed.

Typically, the wake behind a wind turbine is divided into two sections; near wake and far wake, where the boundary between the two sections is difficult to exactly determine. However, the end of the near wake is considered to be where the shear layer reaches the wake axis [11]. Crespo has concluded in his previous work [8] that this normally occurs at around $2-5$ D. In the far wake, the velocity deficit gradually decays downstream of the turbine, and the wake is fully developed. Consequently, axis-symmetry and thus a self-similar wake structure can be assumed [11].

There are several types of models that describe the wake characteristics. Theoretical models,

or kinematic models, are based on self-similar velocity deficit profiles. The momentum equation is used to model the velocity deficit of the wake and the wake growth rate, which is calculated by using information about the different turbulence involved. Examples of these models are, among others, proposed by Lissaman [2], Voutsinas et al. [3] and Vermeulen [4]. Numerical models, or field models, which calculate the characteristics of the flow field at every point, have been, among others, developed by Sforza [5] and Ainslie [10]. Other important models are analytical expressions that calculate the wake parameters, which are based on experimental results rather than theoretical formulation. These expressions are an alternative to the methods mentioned above for controlling a wind farm as they are fast methods and do not require high computational power. For a detailed review of the different wake models see Crespo et al. [8].

As the wake of a wind turbine influences the downstream wind turbines in a wind farm, it is of interest to find a good estimation of how the wake develop. In this thesis, an analytical expression from Schlichting [7], which was derived in order to describe the wake behind by blunt bodies, is studied in order to evaluate if the model is also applicable to predict wind turbine wakes. In addition, three analytical models to predict the turbulence intensity development downstream the wake are analyzed.

2. Wake models

2.1. Velocity decay and Width development model

In the following section, the work by H. Schlichting, Boundary Layer Theory [7], which describes with simple analytical expressions the width and the velocity decay evolution of the wake behind blunt bodies is considered. A wake is created behind a solid body when it is introduced to a fluid flow. The body experiences drag, which generates a loss of momentum, and as a result the velocity of the flow in the wake is reduced.

The studied model is constrained to free turbulent flows, where the laminar friction can be neglected due to a much higher turbulent friction [7]. It is additionally assumed that the pressure across the wake remains constant. Consequently, this assumption is only valid from a certain distance away from the body, limiting the model to the far wake. The model is derived from the boundary layer equation for incompressible flow.

The results from the derivation are the analytical expressions that describe the width and the velocity decay, which are presented in table 1.

Type of flow	Width	Velocity
Two-dimensional wake	$x^{1/2}$	$x^{-1/2}$
Circular wake	$x^{1/3}$	$x^{-2/3}$

Table 1: Analytical expressions for the calculation of width and velocity decay in terms of downstream distance from the blunt body [7].

Two parameters need to be defined in order to comprehend the model derived by Schlichting. The first parameter is the *velocity decay* (u_1), which is defined as the difference between the free stream flow velocity (U_∞) and the velocity at the measured point (U); $u_1 = U_\infty - U$. The second parameter is the *half depth width* ($b_{1/2}$), defined as the width of where the wake has the half of the velocity decay. The reason for defining this parameter is due to the asymptotic behavior of the wake at the edges, which makes it difficult to determine the end of the wake.

To be able to apply the model for different geometries and compare the results, the expressions for $b_{1/2}$ and u_1 are normalized. Consequently, $b_{1/2}$ is normalized by the diameter of the blunt body, giving the expression

$$\frac{b_{1/2}}{D} = C_b \cdot \left(\frac{x}{D}\right)^{1/3} \tag{1}$$

and u_1 is normalized by the inlet velocity, giving

$$\frac{u_1}{U_\infty} = C_u \cdot \left(\frac{x}{D}\right)^{-2/3} \tag{2}$$

where C_b and C_u are proportional constants of $b_{1/2}$ and u_1 respectively, x is the downstream distance behind the turbine and D is the diameter of the blunt body. For the investigated case of a wind turbine wake, D refers to the diameter of the wind turbine rotor. The constant C_b is calculated by plotting experimental values of normalized $b_{1/2}$ against the normalized distance, both in a logarithmic scale. This creates a linear line, which equation is calculated. Concurrently, the analytical expression that defines the width, showed in table 1, is used for calculating $b_{1/2}/D$. Rewritten as $ln(b_{1/2}/D) = ln(C_b) + \frac{1}{3}ln(x/D)$, which has a similar distribution of a linear equation. Equating both intercept terms, the line and the rearranged power law, the parameter C_b can be determined. The same procedure is used to calculate the parameter C_u.

The expression derived by Schlichting to calculate the velocity distribution is

$$\frac{u_1}{U_\infty} = \frac{\sqrt{10}}{18\beta} \cdot \left(\frac{x}{C_D d}\right)^{-1/2} \cdot \left\{1 - \left(\frac{z}{b}\right)^{3/2}\right\}^2 \tag{3}$$

where β is the mixing length factor that is experimentally determined, C_D is the drag coefficient, d is the diameter of the cylinder, z is transverse position in the wake, and b is the width of the wake.

Notice that equation 3 was originally derived for a two-dimensional wake. However, L. M. Swain [9] investigated the circular wake and concluded that the same expression can be applied if the coefficients of the power laws were modified. In this study, the wake of a model wind turbine is investigated and thus, a circular wake is explored, the modified power laws presented in table 1 are being used. Thus, the expression used for the velocity distribution is:

$$\frac{u_1}{U_\infty} = \frac{\sqrt{10}}{18\beta} \cdot \left(\frac{x}{C_T A}\right)^{-2/3} \cdot \left\{1 - \left(\frac{z}{b}\right)^{3/2}\right\}^2 \tag{4}$$

A in this formula refers to the rotor swept area and C_D is replaced by the thrust coefficient of the turbine (C_T).

2.2. Turbulence intensity models

Three models are investigated in order to describe the downstream turbulence intensity development. It is important to predict the turbulence intensity to avoid the fatigue loads produced by the velocity fluctuation in the wake of the upstream turbine. Turbulence intensity is defined as the velocity fluctuation over the mean velocity.

$$TI = \frac{u}{u'} \tag{5}$$

The analyzed models are based on correlations from wind tunnel experiments or measurement field campaigns. The turbulence intensity created by the wind turbine it is estimated and added to the ambient turbulence.

2.2.1. Crespo Model Crespo and Hernandez [20] developed a model for the turbulence intensity created by the turbine. The expression was obtained by fitting with numerical results. The model is only valid for the far wake, as in the near wake an expansion occurs which is not considered in the model.

$$\Delta I \;=\; 0.73\; a^{0.83}\; I_{\infty}^{-0.0325}\; \left(\frac{D}{x}\right)^{0.32} \tag{6}$$

where the parameters a and I_{∞} according to the theory should be between $0.1 < a < 0.4$ and $0.07 < I_{\infty} < 0.014$

2.2.2. Quarton Model A model was developed by Quarton [18] to describe the turbulence intensity development behind a wind turbine. The model is based on the Crespo model (se section 2.2.1) which correlations are improved by fitting with experimental results, both wind tunnel and field experiments.

$$\Delta I \;=\; 4.8\; C_T^{0.6}\; I_{\infty}^{0.68}\left(\frac{\chi_N}{x}\right)^{0.57} \tag{7}$$

where C_T is the drag coefficient and χ_N is the near wake length, usually ranging between 1 D - 3 D

2.2.3. Frandsen Model Frandsen and Thogersen [21] during the study of the fatigue in wind turbines, developed a expression for the turbulence intensity based on measurements, where the constants are chosen to best fit with the data.

$$\Delta I = \frac{1}{1.5 \;+\; 0.3\;(x/D)\;\sqrt{V_{hub}}} \tag{8}$$

where V_{hub} is related to the parameter C_T.

3. Experimental setup

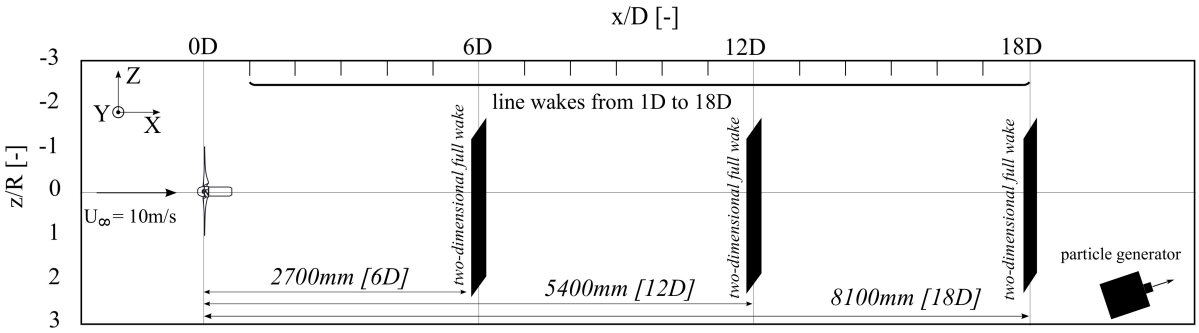

Figure 1: Non scaled sketch of the experimental set up in the wind tunnel.

The experiment in this study was carried out in the wind tunnel at the Department of Energy and Process Engineering at the Norwegian University of Science and Technology (NTNU). A simple sketch of the experimental setup is presented in figure 1. The wind tunnel has a cross sectional area (zy-plane) of 2.7 m × 1.8 m and a length (x-axis) of 11 m. The turbine, which has a rotor diameter (D) of 0.45 m, was installed at a distance 2.71 D downstream of the inlet of

the wind tunnel. The hub height was adjusted to 1.97 D (0.89 m) to have the rotor in the center of the cross section. The inlet velocity (U_∞) was set to 10.0 m/s and kept constant during the wake measurements. To ensure this, the velocity of the incoming flow was measured for every measurement point using the pressure difference at the contracted duct at the wind tunnel inlet. The low turbulence inflow condition has an ambient turbulence intensity (TI) of 0.23%. Additionally, by including a grid at the inlet of the wind tunnel, a higher ambient turbulent inflow condition is achieved, with a value of 10.5%. The grid is formed by even distributed quadratic wooden spars of 47 mm side length leading in a mesh size of 240 mm space between them. providing a uniform flow profile. In order to have uniform flow conditions along the x-axis, the roof of the test section was adjusted for a zero pressure gradient in the streamwise flow direction. Consequently, the mean velocity in the empty tunnel is found to be uniform within $\pm$ 0.6% [16]. A two-component Laser Doppler Velocimetry (LDV) probe, which was used to measure the velocity components, was mounted onto a traverse in order to move the LDV probe in the wind tunnel. In order for the LDV probe to detect the airflow, a small smoke machine generating particles with a size of 0.5-2.0 μm was placed in the far back of the wind tunnel. As the wind tunnel is of the type closed-loop, the particles were evenly distributed in the airflow during the returning process. 50 000 samples measured with the LDV probe were collected at every measuring point, resulting in an uncertainty of 7.3% in the measurements.

Figure 2: Picture of the test section with LDV probe mounted onto the traverse and the wind turbine and the grid installed.

Three two-dimensional full wakes in the zy-plane were measured at distances in the x-direction of 6 D, 12 D and 18 D behind the turbine. The measured cross sectional area for the full wakes was ranging from -1.33 D to 1.33 D in z-direction, and from -1.07 D to 1.07 D in y-direction, with the center located at the rotor axis. With an increment of 0.13 D (0.06 m) in both directions, a measurement grid consisting of 357 points was investigated. In addition, line wake measurements were performed at every distance D from the turbine, ranging from 1 D to 17 D, at a center line 0.22 D (0.10 m) below the rotor axis. The z-axis remained the same, ranging from -1.33 D to 1.33 D, as well as the increment size, 0.13 D. For the experiments with low turbulence ambient condition, the height for the line wake measurements was chosen at a lower y-value than the rotor axis due to the center of the wake shifted downward behind the turbine, which

was observed from the full wake measurements which are presented in detail in chapter 4. In the case of high turbulent ambient condition, the line wake measurements were performed at hub height as the wake center was not shifted downwards.

3.1. Turbine

For the presented study a new rotor was developed. The basis of the new rotor design is the rotor developed at the Department of Energy Process Engineering at NTNU Trondheim which is described in detail by Krogstad and Lund [6]. The new rotor is also based on the NREL S826 airfoil, however, the blade parameters are modified to get a smaller rotor diameter. Here, the twist and the chord distribution were not changed, only the increment between the blade elements was halved to also get a rotor radius which has half the radius of the reference rotor. Thus, the new rotor has a diameter of 0.450 m. This smaller rotor was designed to be able to investigate the far wake and thus, a larger range behind the turbine. Furthermore, blockage effects and wake interference with the wind tunnel walls should be as small as possible such that the wake can develop without being contracted. Whereas the reference rotor has a wind tunnel blockage ratio of around 13% the new rotor has only a blockage ratio of around 3%. A higher limit of 10% blockage ratio is suggested to avoid the interference between the measurements and the walls of the wind tunnel [15]. Hence, it is expected that the wake can expand without being influence by the wind tunnel walls too much. The single rotor blades were produced with a 3D printer based on the multi-jet technology and connected at the hub with metal rings. The rotor was mounted on a newly designed turbine test rig, which was developed to have a small nacelle. The assembly in the wind tunnel is shown in figure 2. With this assembly the performance and the thrust for the new rotor were measured. In figure 3, the resulting power coefficient

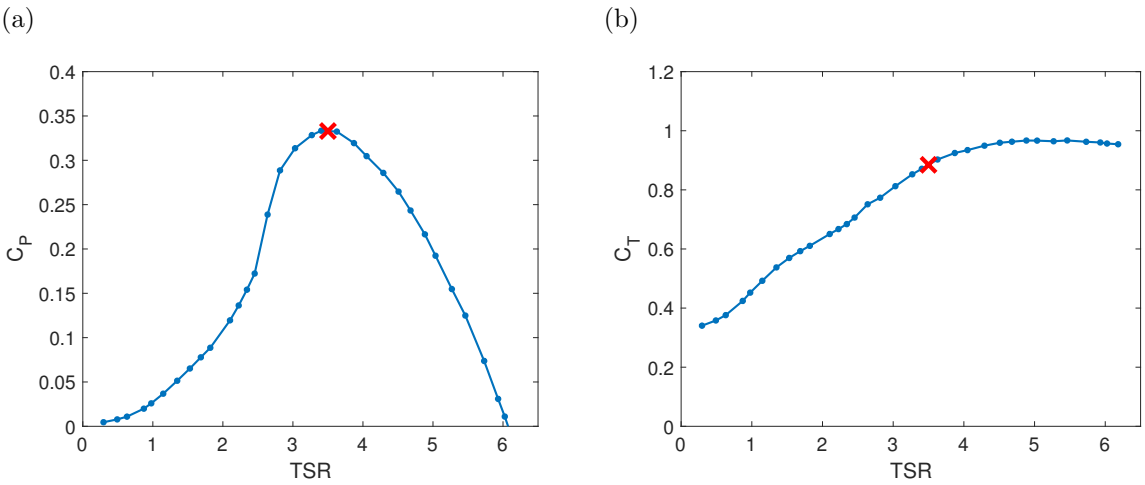

Figure 3: Experimental results for (a) C_p and (b) C_T over TSR. The red X marks the TSR where all the wake measurements were conducted.

(C_P) and thrust coefficient (C_T) are presented. The optimum tip speed ratio (TSR) for the new rotor is 3.5, which is where the turbine reaches the highest power efficiency. This point is marked in figures 3a and 3b by a red cross. All the wake measurements were conducted at this optimum TSR of 3.5. The presented C_T represents the thrust of the rotor only. To separate the rotor thrust from the total thrust, the tower thrust was determined by exposing only the tower without the rotor to the flow. The resulting constant tower thrust was then subsequently subtracted from the thrust for the complete assembly for every TSR to get the rotor thrust. As all the wake measurements were done at the optimal TSR with an inlet velocity of 10.0 m/s,

consequently, the resulting Reynolds number at the tip ($Re_{tip} = 60\,000$) is rather low. However, Chamorro, Arndt and Sotiropolus showed in their study [19] that such low Reynolds numbers could effect the structure of the near wake as the turbulence characteristics in this region are influenced by the aerodynamic of the turbine blades. On the contrary, the flow characteristics of the far wake are rather dominated by the lateral transport and thus the mean velocity in the wake as well as higher order statistical moments show only a weak dependence to the Reynolds number. Consequently, it can be concluded that the small rotor is suited well for far wake investigations.

4. Results

4.1. Velocity deficit in the yz-plane

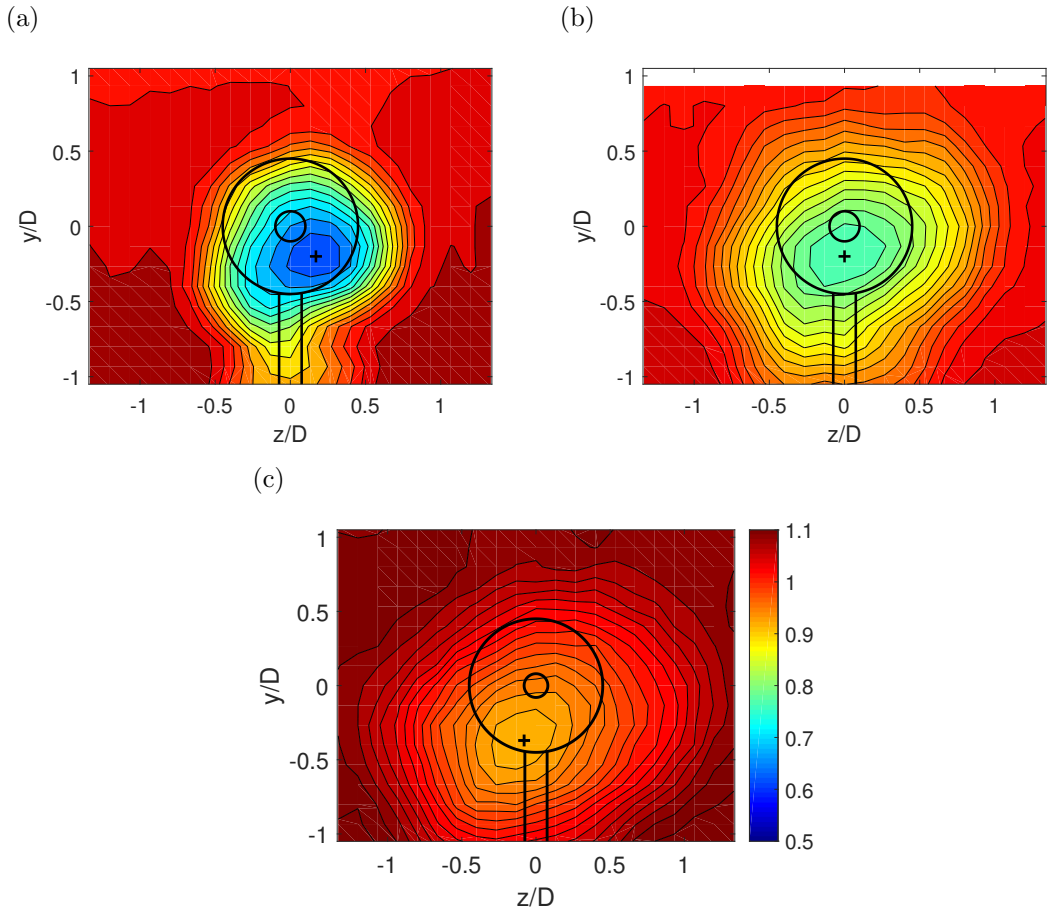

Figure 4: Two-dimensional velocity full wake plots under low ambient turbulence condition in zy-plane at distances of (a) 6 D, (b) 12 D, and (c) 18 D behind the turbine. The plus sign (+) in the plots marks the center of the wake.

In figures 4a, 4b and 4c, two-dimensional contour plots of the full wake under low ambient turbulence conditions in the zy-plane are presented at distances of 6 D, 12 D and 18 D, respectively. As expected, the velocity decay decreases as the wake moves downstream. The evident development of the wake can be seen, with an expansion of the wake as the downstream distance increases. This behaviour was expected, as previous work has already shown the same

wake development [11]. In all three cases, a downshift of the center line of the wake can be observed. This is assumed to be due to interaction of the wake and the turbine tower. An uneven momentum induced by the presence of the tower pushes the wake downwards. The effect was investigated in detail by Pierella [12]. Consequently, the line measurements presented in the following sections were measured at a distance 0.22 D below the rotor axis. This distance was chosen after analyzing the wake and the wake center was defined where the lowest velocities were found. Its position is marked in figure 4 by a plus sign (+).

At 6 D and 12 D, as expected from the observations by Pirealla [12], a slightly larger horizontal expansion can be seen, nevertheless the wakes are approximately circular whereas at 18 D a quite large expansion in horizontal direction can be observed and the wake has a rather oval shape. This is expected to be due to the interference with the traverse in the back of the wind tunnel since, at 18 D, the LDV probe had to be placed beneath the framework supporting the traverse, instead of being placed in front of the framework, which was the case for the other downstream distances. This resulted in a contraction of the cross section and thus, a compression of the flow in y-direction. Hence, there is a clear influence of the framework of the traverse on the wake, and consequently, the measurements at 18 D are not considered in the further evaluation of the analytical Schlichting model.

For the experiments with a high ambient turbulence, the center of the wake remains at hub height, as can be appreciated in figure 5, where the velocity was measured in a small grid of 0.1 D step ranging ±0.25 D in vertical and horizontal directions at hub height, 15 D downstream the wind turbine. Thus, the line measurements for the high ambient turbulence conditions were performed at hub height.

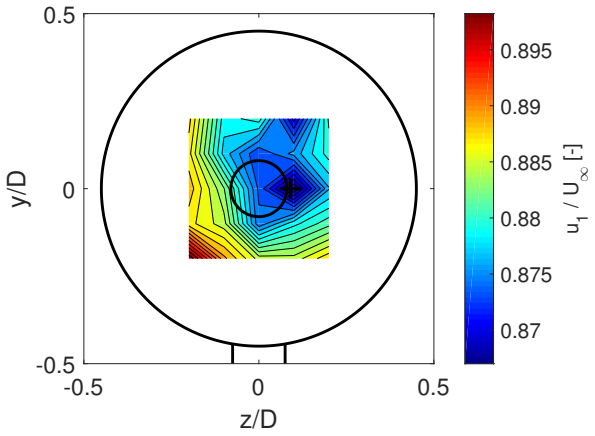

Figure 5: Two-dimenstional velocity wake under high turbulence conditions, centered on the rotor axis 15 D downstream the turbine. The plus sign (+) in the plot marks the center of the wake

4.2. Velocity development in the xz-plane

In order to see how the wake was developing with increasing distance downstream from the turbine, line wakes were measured from 1 D to 15 D. The measured points from the line wakes were interpolated to get a fine grid and thus counters for the velocity in flow direction could be determined. The resulting counter plot of the velocity development for both ambient turbulence condition is shown in figure 6. In both cases, a similar behavior of the wake is observed.

The highest velocity deficit is found in the near wake region, whereas, as expected, the velocities increase with increasing distance due to turbulent mixing. In the near wake, which is where the wake is not yet fully developed and thus, does not has a Gaussian shape, the influence

of the turbine geometry is still dominant and can clearly be observed by the two peaks in the velocity deficit. The near wake is stronger in the case of the low ambient turbulence. In the measured wake, the near wake can be defined as the region from right behind the turbine and downstream to 5 D - 6 D downstream. Whereas for the high ambient turbulence the near wake is reduced to 3 D - 4 D, due to the higher mixing conditions.

However, with increasing downstream distance, the wake is getting more uni-modal and is considered to be fully developed in the far wake, which can be identified by a Gaussian shape.

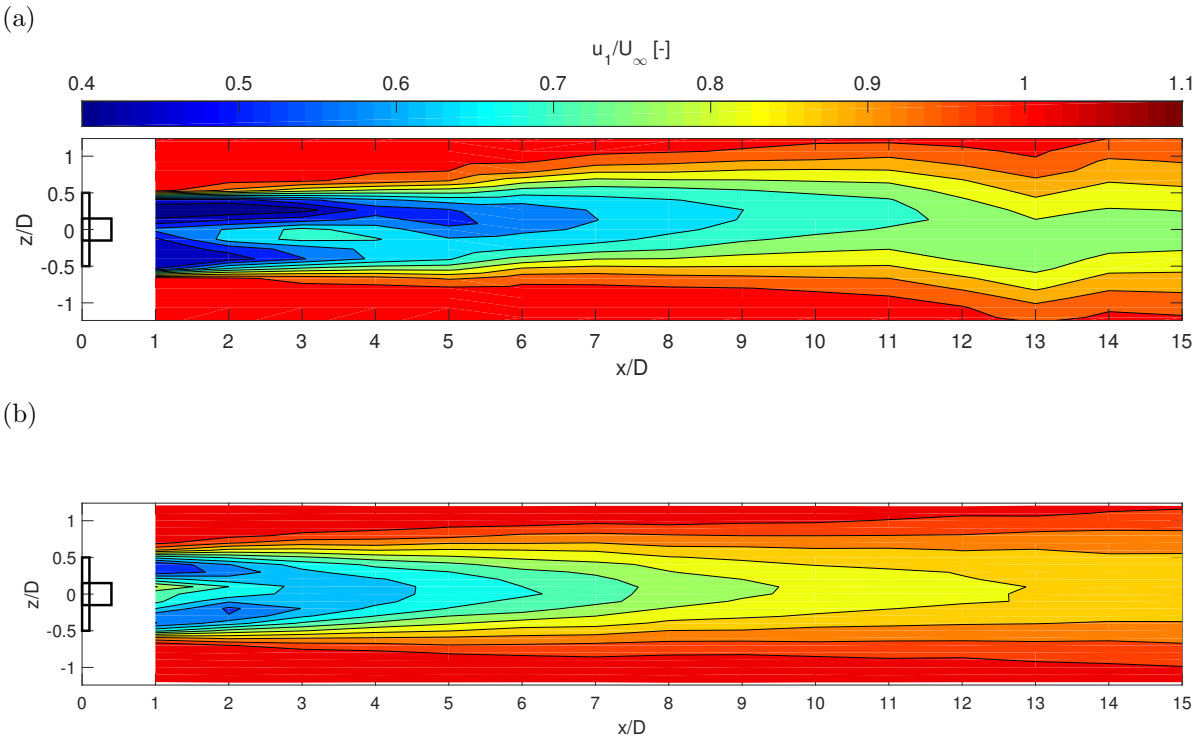

Figure 6: Velocity profiles of the wake in the xz-plane for (a) low ambient turbulent conditions with a center line at y = -0.22 D and (b) high ambient turbulent conditions with a center line at y = 0 D.

4.3. Turbulence intensity development in the xz-plane

In figure 7,turbulence intensity development from 1 D to 15 D for both cases of ambient turbulence intensity is shown. A two peak structure is observed in the near wake, which corresponded to the tip vortices [17]. In figure 7b, where the ambient turbulence intensity is higher, due to turbulent mixing, those two peak structure moved less further downstream the turbine compared with the low ambient turbulence intensity. The turbulence intensity is reduced as the downstream distance is increased. This recovery of the turbulence intensity in the wake is faster when the ambient turbulence intensity is higher.

(a)

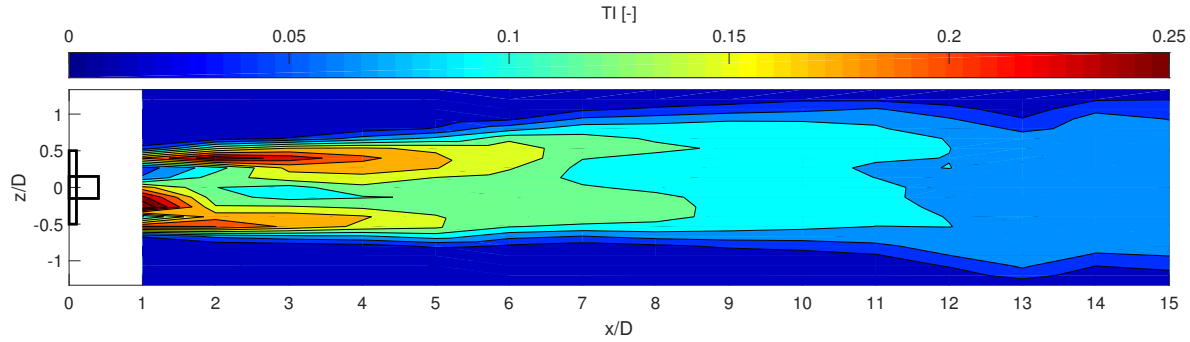

(b)

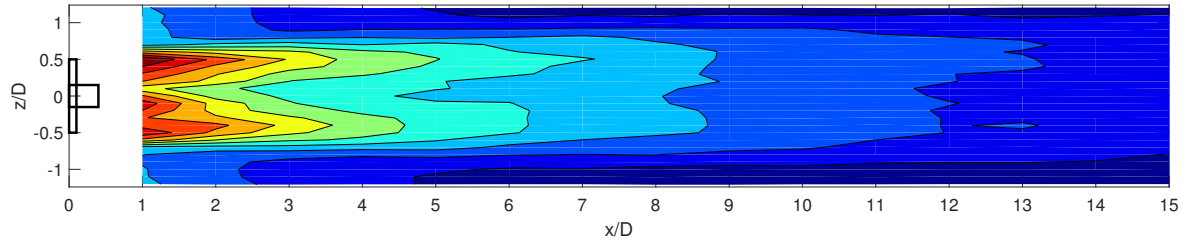

Figure 7: Turbulence intensity profiles of the wake in the xz-plane for (a) low ambient turbulent conditions with a center line at y = -0.22 D and (b) high ambient turbulent conditions with a center line at y = 0 D.

5. Discussion

5.1. Velocity decay

The velocity development of the experimental results analyzed in the previous chapter already suggests, that the analytical model derived by Schlichting seems to represent the far wake regime of a wind turbine very well. The velocity deficit in low ambient turbulence conditions depicted in figure 8a shows that the far wake begins approximately at a distance of 6 D, when the wake shows a Gaussian shape, meaning that the wake is fully developed. This is slightly later than suggested by Crespo et al. [8] who estimates the end of the near wake region between 2 and 5 diameters downstream of the turbine. A reason for this behaviour could be the low turbulent inflow, described in section 3, that results in less turbulent mixing of the wake and thus, longer distances before the wake is fully developed [11]. As the analyzed Schlichting model is asymthotic and thus has not such a good performance at low distances, the results at the distances 5 D and below are not considered in the comparison analysis. With high ambient turbulence conditions, which can be seen in figure 8b, the near wake is ends aproximately at a distance of 4 D, which belongs to the expected range that Crespo [8] suggested. In this case, the distances under 3 D and below are discarted in the analysis. In figure 8, the experimental results of the normalized velocity decay of the line wakes from 6 D to 17 D are compared to the velocity deficit calculated using formula 2.

The measurement for both ambient turbulence conditions results correspond very well with the theoretical line. As Schlichting's model behaves asymptotically, the performance is expected to be improved with increasing downstream distances. However, due to measurement uncertainty a small random spread of the measurement points around the line can be observed. Nevertheless

(a) (b)

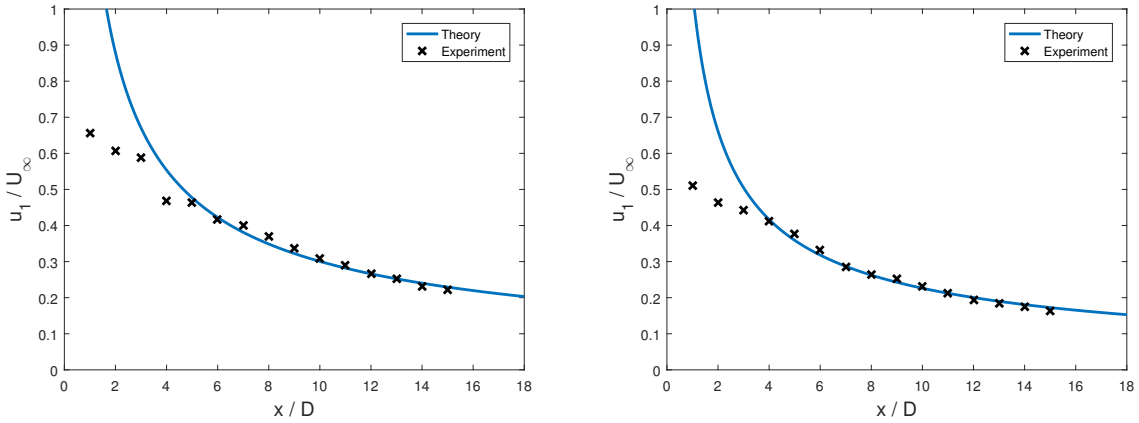

Figure 8: Comparison of the normalized velocity decay for the experimental results and the analytical model for (a) low ambient turbulent conditions and (b) high ambient turbulent conditions.

the average deviations are only around 1.9% and 2.46% for the low and high ambient turbulence conditions respectively.

5.2. Width development

The comparison between experiments and theory for the development of the width is presented in figure 9. Here, almost the same trend as for the velocity deficit can be observed. In the far wake, 6 D and 4 D for low ambient turbulence and high ambient turbulence respectively, and downstream the experimental results fit very well with the theoretical development of the width and a random distribution of the measured values around both graphs can be seen. The average deviations are of the same order of magnitude as for the velocity deficit, only around 2.25% for the low ambient turbulence condition and 2.84% for the high ambient turbulence condition.

5.3. Velocity distribution

The velocity distribution along the z-axis at different downstream distances is shown in figure 10. To avoid an offset between the experimental and analytical results due to accelerated flow outside of the wake, the velocity in the wake was normalized with the velocity outside the wake for every measurement. Thus, U_∞ was selected to be around 10.3 m/s instead of the constant inlet flow velocity U_∞ of 10.0 m/s. That way, negative values in the outer area of the wake could be avoided, and the theoretical graph could be compared better to the values resulting from the experiments.

The wake profile resulting from the measurements show a similar shape at all different distances. When comparing them to the theoretical velocity profile it can be seen that the theory does not exactly describe the velocity distribution at the edges of the wake $|z/b_{wake}| > 0.70$ as the deviation is over 50% at all distances. However, it should be clarified that these derivations are not relevant, as the order of the magnitude is very small in that region and even very small differences create large deviation that are not significant. Thus, only the inner region of the distribution is considered. In the inside of the wake $|z/b_{wake}| < 0.70$, the deviation is reduced to an average deviation of around 11.3%. Whereas the clearest distinctions can be observed in the center of the wake, where the experimental results tend to form a shallower peak than the wake resulting from the theory. Here the velocity distribution at 6 D shows the highest

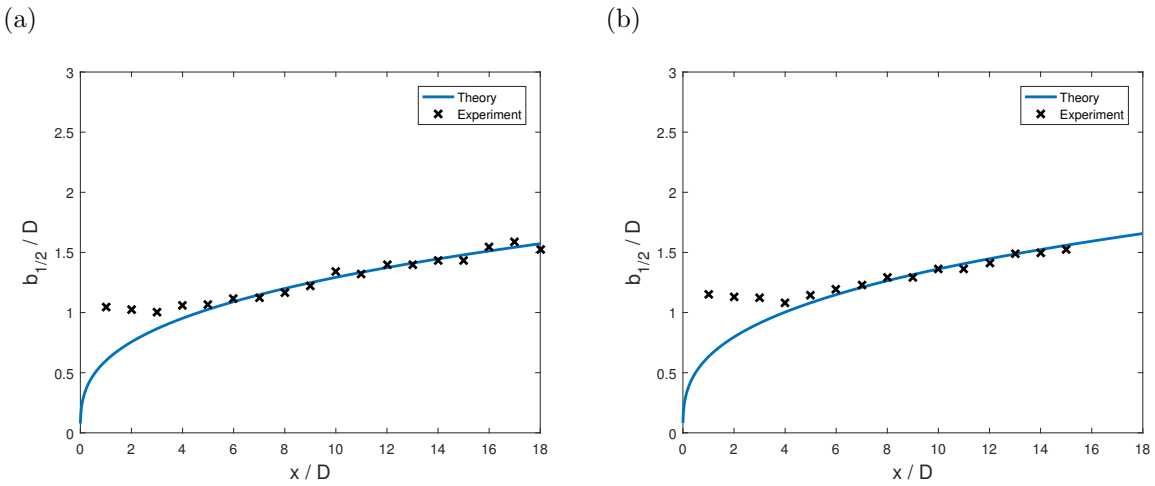

Figure 9: Comparison of the normalized width development for the experimental results and the analytical model for (a) low ambient turbulent conditions and (b) high ambient turbulent conditions.

differences from the theory, which was expected as the the model is asymptotic and thus has it worst performance at low distances.

The velocity distributions from 6 - 15 D show a similar profile, which has a Gaussian shape, meaning that the wake in the far wake regime has self-similarity behaviour [13], as the velocity is distance independent from the turbine. The analytical model is well suited to estimate the shape of the velocity profile in the far wake.

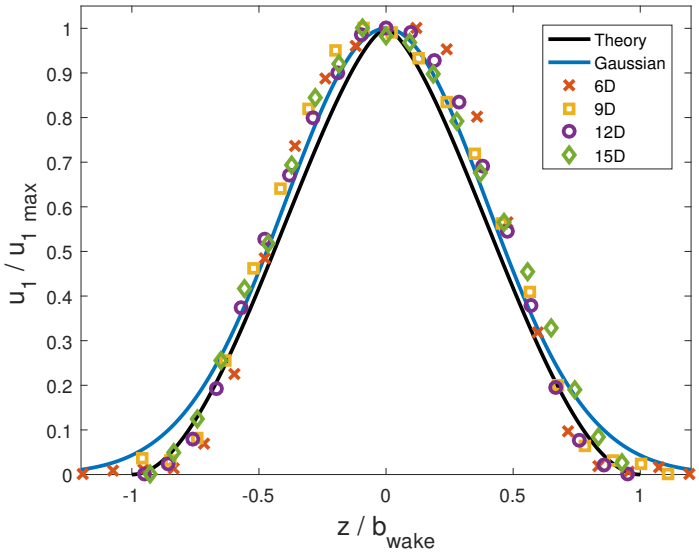

Figure 10: Comparison of the wake shape from the analytical model and velocity measurements at 6 D, 9 D, 12 D and 15 D.

5.4. Turbulence intensity

Three analytical models for turbulence intensity of the wake (Crespo, Quarton and Frandsen) are compared with experimental data. The case of low turbulence intensity was discarded as the turbulence is an unrealistic value (0.23%). The case of high ambient turbulence intensity can be compared to an offshore situation. In figure 11 the comparison between the prediction of the models and the measurements under high ambient turbulence condition is shown. The measurement point is chosen at the maximum turbulence intensity for each measured distance. Similar trend is observed in the three models. The Quarton model is the most accurate with an average deviation of 2.65%, follow by Crespo and Frandsen with 9.01% and 11.32% respectively. It is expected that the Quarton model performs better that Crespo as it is an improvement version.

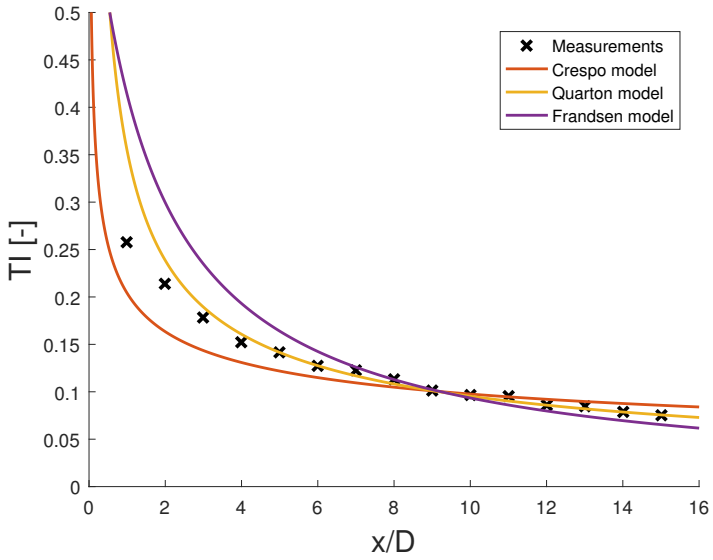

Figure 11: Comparison of the turbulence intensity development of the experimental result with the analyzed models under high turbulent intensity conditions from 1 D to 15 D behind the turbine.

6. Conclusion

An analytical wake model derived for blunt bodies was investigated for the application of the prediction of the velocity decay and width development for wind turbine wakes. Results of the analytical expressions were compared to experimental results of the wake formed behind a model wind turbine. Correlations for the added turbulence intensity were investigated. The theoretical results for the velocity deficit, the wake width and the turbulence intensity are in good agreement with the experimental results. For the investigated parameters in the Schlichting model the deviations between experiments and theory are in the range of only 2% in the analyzed far wake region. Also the Gaussian shape of the velocity deficit in the far wake regime of a wind turbine rotor can be predicted fairly well by the analytical model. A scattered results from the turbulence intensity models are obtained with a deviation between 3 and 10%. Consequently, it can be concluded that the investigated theory derived by Schlichting, which was originally derived for blunt bodies, is applicable to predict the wake of a wind turbine rotor. Also models for describe the turbulence intensity perform fairly well.

Acknowledgments
I would like to thanks my supervisor Lars Sætran which gave me the opportunity to do this thesis. Also, thanks to Franz Mühle and Mari Vatn for their helpful comments.

References

[1] Wiser R H and Bolinger M 2016 *2015 Wind technologies market report*
[2] Lissaman P B S 1979 Energy effectiveness of arbitrary arrays of wind turbines *J Energy* **3**(6) 323-8
[3] Voutsinas S G, Rados K G and Zervos A 1990 On the analysis of wake effects in wind parks *J Wind Eng Ind Aerod* **14** 204-19
[4] Vermeulen P E J. 1980 An experimental analysis of wind turbine wakes *3rd Int Symp on Wind Energy Systems* Lyngby 431-50
[5] Sheerin P M, Sforza and M. Smorto 1981 Three-dimensional wakes of simulated wind turbines *AIAA J* **19**(9) 1101-7
[6] Krogstad P Å and Lund J 2012 An experimental and numerical study of the performance of a model turbine. *Wind Energy* **15**(3) 443-57
[7] Schlichting H 1979 *Boundary Layer Theory* McGRAW-HILL series in Mechanical Engineering 7th
[8] Crespo A, Hernández J and Frandsen S 1999 Survey of modelling methods for wind turbine wakes and wind farms *Wind Energy* **2**(1) 1-24
[9] Swain L M 1929 On the turbulent wake behind a body of revolution *Proc. R. Soc. A* **125**(799) 647-59
[10] Ainslie J F 1988 Calculating the flow field in the wake of wind turbines *J Wind Eng Ind Aerod* **27**(1) 213-24
[11] Sanderse B 2009 Aerodynamics of wind turbine wakes - literature review Report ECN-E-09e016
[12] Pierella F and Sætran L 2017 Wind tunnel investigation on the effect of the turbine tower on wind turbines wake symmetry Paper accepted for publication in *Wind Energy*
[13] Gratton J 1991 Similarity and self similarity in fluid dynamics *FCPH* **15** 1-106
[14] Helmis CG, Papadopoulos KH, Asimakopoulos DN, Papageorgas PG, Soilemes AT. 1995 An experimental study of the near wake structure of a wind turbine operating over complex terrain *Solar Energy* **54**(6) 413–28.
[15] De Vries O. 1983 On the theory of the horizontal-axis wind turbine *Ann Rev Fluid Mech* **15** 77-96
[16] Bartl J and Sætran L 2017 Blind test comparison of the performance and wake flow between two in-line wind turbines exposed to different turbulent inflow conditions *Wind Energ Sci* **2** 55-76
[17] Schepers J G, Obdam T S and Prospathopoulos J 2012 Analysis of wake measurements form the ECN Wind Turbine Test Site Wieringemeer EWTW *Wind Energy* **15** 575
[18] Quarton, DC. 1989 Characterization of wind turbine wake turbulence and its implications on wind farm spacing *Department of Energy of the UK* ETSU WN5096
[19] Chamorro L.P., Arndt R. and F. Sotiropoulos 2012 Reynolds number dependence of turbulence statistics in the wake of wind turbines *Wind Energy* **15**(5) 733-742
[20] Crespo, A. and Hernandez, J. 1996 Turbulence characteristics in wind turbine wakes *J Wind Eng Ind Aerod* **61** 71-85
[21] Frandsen, S Thøgersen, ML. 1990 Integrated fatigue loading for wind turbines in wind farms by combining ambient turbulence and wakes. *Wind Eng* **23** 327-40